Received: 8 December 2023 | Revised: 24 January 2024 | Accepted: 29 February 2024 | Published online: 4 March 2024

RESEARCH ARTICLE

Archives of Advanced Engineering Science
2026, Vol. 4(1) 25–32
DOI: 10.47852/bonviewAAES42022250

BON VIEW PUBLISHING

Anti-roll Bar Optimization of an Urban Electric Bus

Merve Alpar[1], Efe Savran[2] and Fatih Karpat[3,*]

[1]*Chassis Systems, Karsan Automotive, Türkiye*

[2]*Powertrain, Karsan Automotive, Türkiye*

[3]*Mechanical Engineering Department, Bursa Uludag University, Türkiye*

Abstract: Stiffness and stability are of high importance for vehicles. Existing suspension systems are working for vehicle stability increasing and they are not limited to own. One of the stability increaser extra elements is the anti-roll bar. The anti-roll bar is a suspension system supporter in vehicles. However, bar stiffness plays a critical role in vehicle stability. Bar stiffness can be managed on the predefined limitations. Therefore, a light, effective, and reliable vehicle system can be obtained. In this study, an urban electric bus anti-roll bar optimization was conducted numerically. For optimization, the bar diameter was changed between 25 mm and 40 mm. S235, 50CrV4, AISI 1065, and AL 7075 were selected for material comparison. According to vehicle stability limitations under the lateral 1 m/s^2 acceleration, different bar diameters and material specifications were analyzed with the finite element method. Results of this study showed that the highest stiffness and the lightest bar can be achieved with a 36 mm diameter and AISI 1065 steel combination. Obtained results can lead to vehicle stability studies in the future.

Keywords: anti-roll bar, design refinement, finite element analysis, mechanical resilience

1. Introduction

Anti-roll bar, also known as a stabilizer bar, is a vehicle stability and stiffness increaser [1] element whose general material is steel and prevents the vehicle from tipping over due to high roll angles that occur during cornering [2]. The geometry of the parts may vary depending on the placement of the parts where they are used. During cornering, the vehicle's center of gravity shifts widely toward the cornering wheels, so a rotation angle on the linear axis will occur on the vehicle body. Thanks to correctly selected anti-roll bars, the vehicle body's bending during cornering will remain within the specified limits, road holding will increase, and passenger comfort will be kept at the desired level. Anti-roll bars are parts that are mechanically exposed to torsional stress. Therefore, it only supports rotational movements in the longitudinal axis of the vehicle.

Finite element analysis is a numerical method frequently used in various fields. The process begins with breaking down a structure into more easily solvable unit elements and ends with obtaining answers under specified boundary conditions. The responses received from the structure include basic values such as stress distribution, deformation amount, and reaction forces. Effective solutions can be produced in studies such as optimization, weight reduction, and improvement. Finite element analysis can produce highly accurate results with the help of a mathematical approach.

The correct selection of material and shape is effective in the design of an optimum part [3]. Optimization involves the approach of determining the difference between the ideal target to be achieved in a structure or a system under consideration and the existing structure and eliminating this difference under various conditions. Topology optimization studies are carried out to reduce weight in a structure that is under a certain mechanical load. In terms of the automotive industry, driving behavior or vehicle system optimization is carried out to optimize the energy consumption of a vehicle. The case that is brought closer to the ideal determined as a result of optimization will be more useful in terms of use.

There are several anti-roll bar design and optimization studies literature [2, 4–10]. In this study, the diameter and material optimization of an anti-roll bar was carried out numerically. Finite element analysis was used in the study. In the analyses, the condition that the load acting on the bar is subjected to a lateral acceleration of 1 m/s^2 and, as a result, the bar is torsioned due to the lateral bending movement of the vehicle body, is taken into account. The maximum displacement amount was determined according to the lateral acceleration value. In structural analyses, torsion angle, reaction force, and stress distributions were obtained by affecting the maximum displacement value on the bar. Stiffness expressions were derived from the obtained values according to material and diameter values. Combinations with values greater than the target stiffness value were determined and selection was made according to the lowest mass target.

2. Methodology

In this study, which is based on the torsion and bar rigidity of a vehicle's anti-roll bar due to vehicle lateral acceleration, the finite

*Corresponding author: Fatih Karpat, Mechanical Engineering Department, Bursa Uludag University, Türkiye. Email: karpat@uludag.edu.tr

element method was used. For the accuracy of the study, the torsional condition was determined in advance, and the dimensions were finalized both on paper and by the finite element analysis method for a specific sample. After method and condition validation, a mesh convergence study was conducted and unit mesh size was determined. Since the mesh element type, as well as the size, affects the accuracy of the analysis, tetrahedron, hex dominant, and sweep-type mesh were applied to the same part with the same dimensions. Anti-roll bar boundary conditions were determined for finite element analysis under the dynamic impact to which the vehicle is exposed. The mechanical properties of 4 different materials, namely steel and aluminum, which are frequently used industrially, are shared. Figure 1 is a visual summarization of the operating conditions of an anti-roll bar.

Figure 1
Working cases for the anti-roll bar

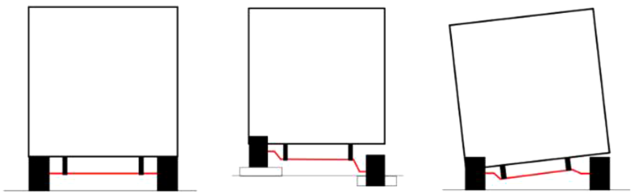

2.1. Study validation

For numerical studies to result in high accuracy, operating conditions must be verified with a reliable approach. Verification can be carried out by a real test or by numerical calculations that are generally known and reliable. This study focuses on the torsion of an anti-roll bar, and before the structural analysis was carried out, a torsion study was carried out on a 50 mm long and 36 mm diameter sample using an 8 mm sweep mesh structure. In addition, the torsion results of the specified part were calculated and compared with the appropriate formulation.

Equations (1) and (2) express the shear stress and moment of resistance occurring in a cylindrical part subjected to torsion.

$$\tau_p = \frac{M_b}{W_p} \tag{1}$$

$$W_p = \frac{I_p}{r_{max}} = \frac{\frac{\pi D^4}{64} * 2}{\frac{D}{2}} \tag{2}$$

Figure 2 shows the torsion calculation made on paper with Equations (1) and (2), realized with finite element analysis.

For 300 Nm torque and 36 mm part diameter, the maximum shear stress can be calculated as 32.75 MPa in the paper. The same condition brings about 32.827 MPa maximum shear stress on the outer surface of the part in finite element analysis with 8 mm sweep mesh and S235 structural steel. Relative error was found as 0.23%. Loading conditions and result images are shared in Figure 2.

Equations (3) and (4) express Hooke's law in a part subjected to torsion condition. Here, shear stress, shear strain, and shear angles can be determined. In Equations, γ is the shear strain, and G is the shear modulus and given as 81000 MPa for S235 in the literature [11]. Figure 3 illustrates the given parameters in Equation (4).

$$\tau_p = G * \gamma \tag{3}$$

$$\gamma = \frac{\Delta l}{l_0} = \frac{r * \varnothing}{L} \tag{4}$$

Equations (5) and (6) [12] show the derivation of the torsion angle from the shear stress.

$$\tau_p = \frac{M_b}{W_p} = G * \gamma \tag{5}$$

$$\varnothing = \frac{M_b L}{G I_p} \tag{6}$$

Twist angle was found as 0.0011236 rad with numerical calculation and found as 0.0011231 rad with finite element analysis. The relative error is near 0.04%. The torsion angle and part are shared in Figure 4.

2.2. Mesh convergence

Mesh convergence is a critical aspect in finite element analysis as it directly influences the accuracy and reliability of simulation results. In finite element analysis, complex structures are separated into smaller elements, forming a mesh that approximates the behavior of the real-world system. Mesh convergence refers to the process of refining this mesh to achieve convergence in the solution, ensuring that further refinement does not significantly alter the results. A converged mesh implies that the solution has reached a stable and accurate representation of the physical behavior of the system.

Figure 2
Boundary condition (left) and maximum stress distribution (right) on the validation part

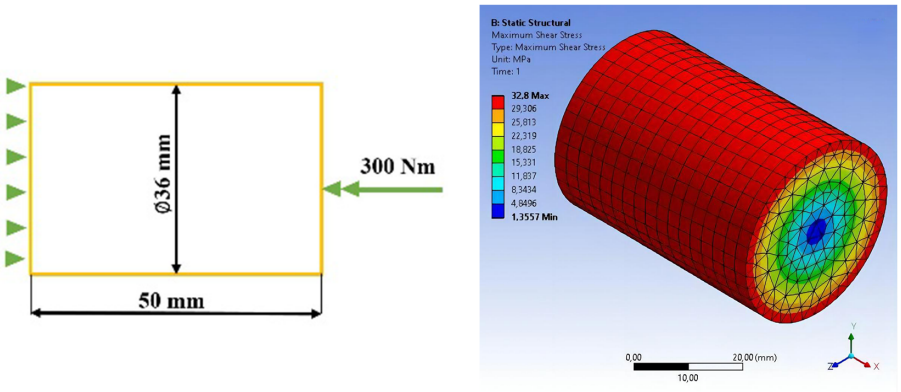

Figure 3
Twist length and angle definition on the part

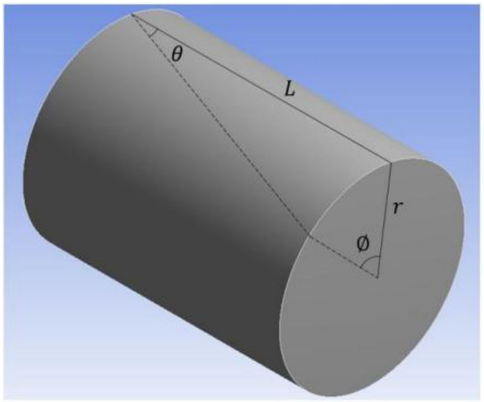

In the mesh convergence of the study, the mesh unit element size was reduced from 10 mm to 1 mm. Ten finite element analysis studies were repeated under the same conditions, and maximum stress values were obtained according to the von Mises criterion. Taking the stress value occurring in the 10 mm mesh unit size as a reference, the difference ratios were calculated based on the stress values occurring in other mesh sizes. Maximum stress values and difference ratios are shared in Figure 5. Based on the stress and difference ratios obtained, it was decided to use an 8 mm mesh unit element size with a difference rate of 0.2%.

According to the situations specified in the section where the appropriate mesh type is selected, skewness and aspect ratio values are created according to unit element sizes at the mesh convergence stage and are shown in Figure 5. According to the previously mentioned mesh evaluation criteria, it appears that the 8 mm mesh size is within the acceptable quality range.

2.3. Mesh type definition

In this part of the study, the appropriate mesh structure was determined. Apart from the mesh unit size, the suitability of the mesh type is also a factor that affects the accuracy of the work to be done. In Figure 6, tetrahedron, hex dominant, and sweep mesh types, whose images are shared and used in many studies, are compared. The results obtained from the finite element analysis study carried out on structures created with 3 different mesh types under the same loading condition are shared in Table 1. According to the mesh evaluation criteria in the literature, the necessary evaluation was made and the sweep mesh was found as the most appropriate for the study. In Table 1, *AR* is the average aspect ratio, *S* is the average skewness, *J* is the Jacobian ratio (MAPDL), and *PT* is the process time.

Table 1
Mesh type comparison table

Mesh type	*AR*	*S*	*J*	*PT* (s)	Used memory (Mb)
Tetrahedron	1.91	0.25	1.03	3	43
Hex dominant	9.04	0.53	2.50	4	62
Sweep	2.10	0.16	1.01	4	215

In a related study [13], mesh quality criteria were specified and the threshold values were expressed as 3 for aspect ratio, 0.45 for skewness, and 0.7 for Jacobian. According to the mesh type comparison results obtained and shared in Table 1, although the sweep-type mesh structure requires longer process time and memory, it was found to be more suitable for this study. Sweep-type mesh was structured with uniform size function, fine relevance center, and slow transition. 21730 nodes and 6630 elements were obtained on the part with a specified mesh combination. The parts to which the mesh types evaluated in the study are applied can be seen in Figure 6.

The sweep mesh with an 8 mm unit element size applied to the anti-roll bar can be seen in Figure 7.

2.4. Application definition

The anti-roll bar subject to the study belongs to an electric vehicle and since it serves in public transportation, passenger comfort is of great importance. For this reason, it is expected that the bar will not exceed the targeted deformation and torsion amounts during the stage of supporting the vehicle structure. In this study, it was requested that the twist at the point where the anti-roll bar is fixed to the chassis should not exceed 0.6° when the vehicle is subjected to a lateral acceleration of 1 m/s^2. The maximum displacement value resulting

Figure 4
Twist angle result (left) and angle surface (right) of the part

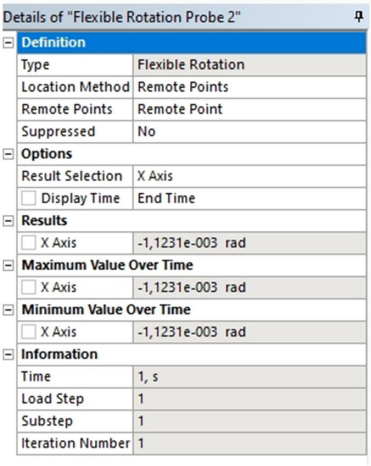

Details of "Flexible Rotation Probe 2"	
Definition	
Type	Flexible Rotation
Location Method	Remote Points
Remote Points	Remote Point
Suppressed	No
Options	
Result Selection	X Axis
Display Time	End Time
Results	
X Axis	-1,1231e-003 rad
Maximum Value Over Time	
X Axis	-1,1231e-003 rad
Minimum Value Over Time	
X Axis	-1,1231e-003 rad
Information	
Time	1, s
Load Step	1
Substep	1
Iteration Number	1

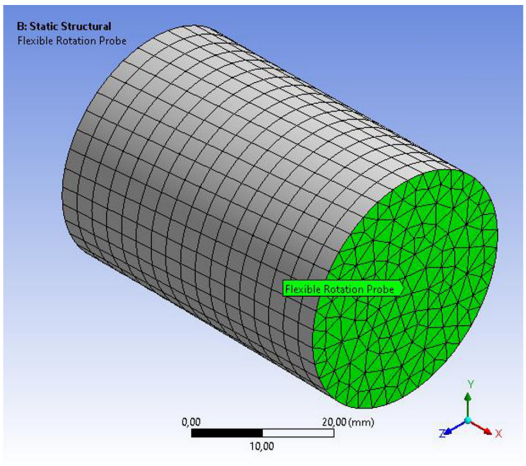

Figure 5
Mesh convergence study graph

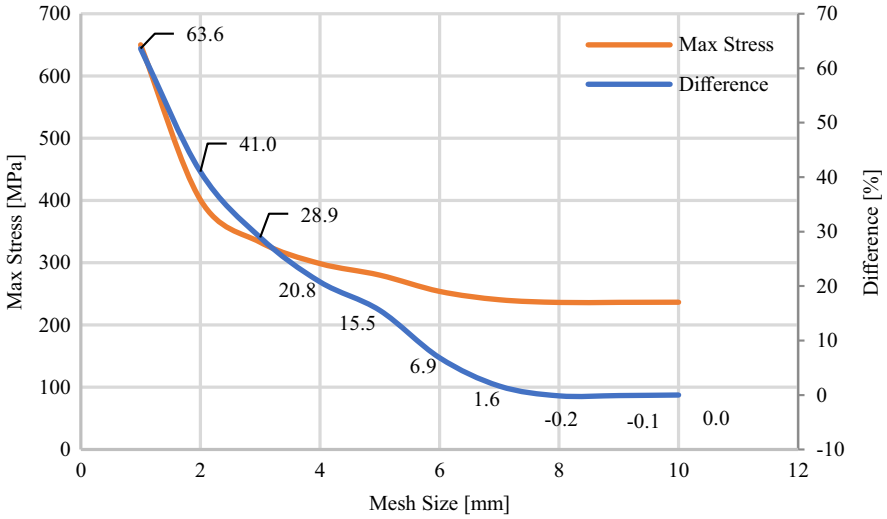

Figure 6
8 mm mesh structure illustrations: (a) tetrahedron, (b) hex dominant, and (c) sweep

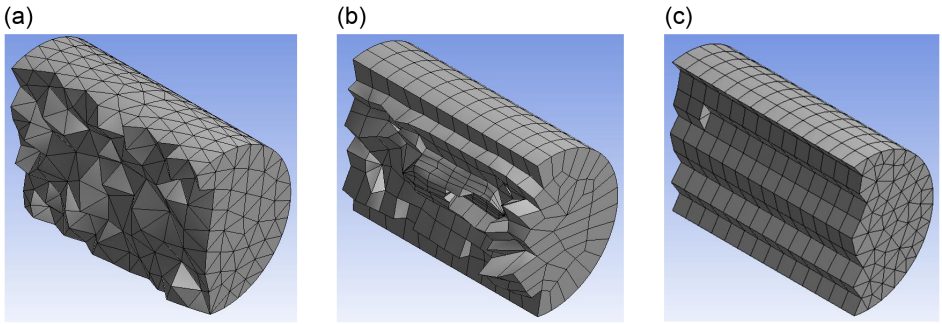

Figure 7
8 mm sweep mesh structured bar

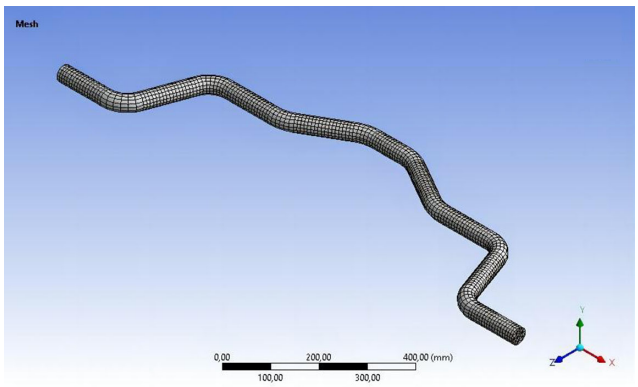

from the specified torsion angle criterion according to the bar dimensions is approximately 6 mm.

As seen in Figure 8, due to the resulting moment, a force of 2219.25 N acts at the junction points of the anti-roll bar with the wheels. The perpendicular measure between the force application surface and chassis connection point is 200 mm. Therefore, the bar cross-sectional area exposed 443.85 Nm torque. According to this information, considering the force value that can create a torsion angle of 0.6° [14] which brings about 6 mm displacement in the force-exposed surfaces, the anti-roll bar is expected to have a stiffness value of at least 739.75 Nm/°.

2.5. Finite element analysis

Finite element analysis is an engineering approach used to simulate and predict the mechanical behavior of structures. It is based on the principle of approximating the physical behavior of the entire structure by dividing a part into smaller elements. Finite element analysis is frequently used in a variety of engineering disciplines, including automotive, construction, aerospace, and materials science. The process involves decomposing a considered geometry into finite elements, applying material properties and boundary conditions, and then solving mathematical equations to predict how the structure will respond to different loads and environmental conditions. With the help of finite element analysis, designs can be optimized, structural integrity can be evaluated, and possible problems can be identified to provide more efficient and

Figure 8
Load case for anti-roll bar

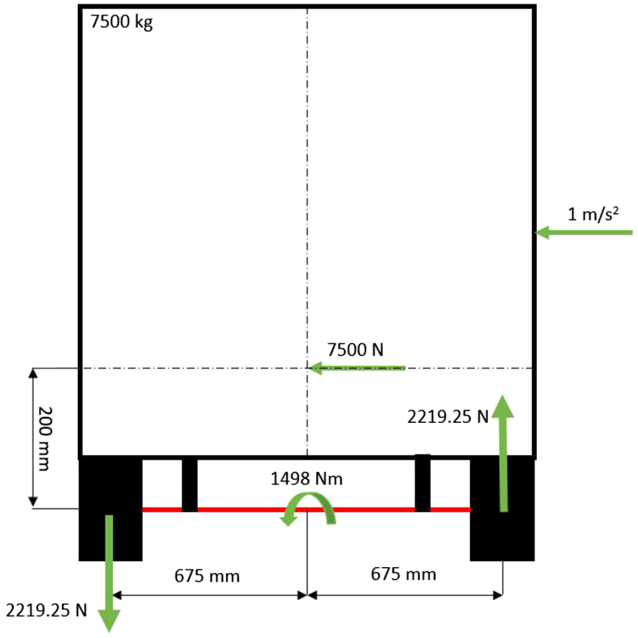

cost-effective engineering solutions. Matrix formats are used in finite element analysis static solutions due to the requirement that a mathematical solution process be applied simultaneously for more than one part. Figure 9 shows an example solution matrix [15–17]. It is known that, in basic terms, each part works like a spring and has a rigidity according to its structure, and as a result of the effects on it, the displacement result is obtained depending on the structural rigidity. With this result, results such as stress, displacement, and torsion angle can be obtained on the structure.

In the finite element analyses of the study, torsion analyses were performed for an anti-roll bar. As the application conditions were previously stated, the stiffness values of the structure were obtained according to different diameters and materials, and the combination with which the target stiffness and above could be achieved was determined. For this target, the structure was moved diagonally from the edge regions by 6 mm on the y-axis. On the other hand, since there is freedom for rotational movement in the connection areas of the bar with the chassis, cylindrical support is defined in these areas. In Figure 10, areas of *A* and *B* are cylindrical support in blue color, and *C* and *D* are displacement applied areas in yellow color.

Figure 9
Finite element analysis static analysis solution system

$$\begin{bmatrix} \frac{AE}{L} & 0 & 0 & 0 \\ 0 & \frac{12EI}{L^3} & \frac{6EI}{L^2} & 0 \\ 0 & \frac{6EI}{L^2} & \frac{4EI}{L} & 0 \\ 0 & 0 & 0 & \frac{GJ}{L} \end{bmatrix} * \begin{bmatrix} u \\ v \\ \theta \\ \emptyset \end{bmatrix} = \begin{bmatrix} F \\ Q \\ M \\ T \end{bmatrix}$$

Figure 10
Finite element analysis boundary condition

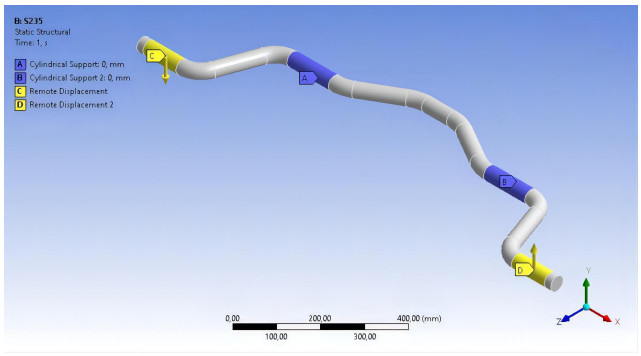

2.6. Material

Material selection is as valuable as a suitable dimension definition for mechanical parts. Suitable material property provides good mechanical behavior and reliable parts. For the anti-roll bar study, S235 [11], 50CrV4 [18], AISI 1065 [19], and Al 7075 [20] materials which are most seen in literature were selected to compare. The chosen material group includes 3 steel and an aluminum alloy. Steel materials are mostly used in industry and also are suitable for several applications. Aluminum alloys are good materials for lightweight projects and mass is an energy consumption effective parameter on the vehicles. Therefore, aluminum was chosen for mass reduction besides the steel materials. The mechanical properties of the chosen materials are given in Table 2.

3. Results

According to the finite element analyses performed for different diameters under the specified conditions, the equivalent maximum stress, torsion angle, and reaction forces with the von Mises criterion were obtained. Bar stiffness was obtained from the obtained force and torsion angles. Safety coefficients were obtained based on the maximum stress values according to the tensile yield strength values between the mechanical properties of the materials. Obtained torsion angles were considered reasonable for relative study [21]. Mass values were also found for lightness evaluation. Obtained data from finite element analyses are shared in Tables 3, 4, and 5. Also, calculated stiffness values, mass data, and safety factors are given in Tables 6, 7, and 8.

Table 2
Mechanical properties of materials

Property	S235	50CrV4	AISI 1065	AL 7075
Density (kg/m^3)	7850	7850	7850	2810
Young's modulus (MPa)	210000	210000	200000	71700
Poisson's ratio	0.3	0.3	0.3	0.33
Tensile yield strength (MPa)	250	1333	490	503
Tensile ultimate strength (MPa)	400	1409	635	572

Table 3
Equivalent maximum stress (MPa) results

Bar diameter	S235	50CrV4	AISI 1065	AL 7075
40 mm	266.45	266.45	253.76	90.45
36 mm	237.57	237.57	226.26	80.62
34 mm	220.19	220.19	209.70	74.74
32 mm	212.69	212.69	202.56	71.30
30 mm	196.70	196.70	187.33	66.70
28 mm	181.93	181.93	173.26	61.71
25 mm	158.81	158.81	151.25	53.76

Table 4
Rotation (degree) results

Bar diameter	S235	50CrV4	AISI 1065	AL 7075
40 mm	0.90130	0.90130	0.90130	0.90358
36 mm	0.90155	0.90155	0.90155	0.90378
34 mm	0.90191	0.90191	0.90191	0.90411
32 mm	0.90183	0.90183	0.90183	0.90400
30 mm	0.90211	0.90211	0.90211	0.90428
28 mm	0.90223	0.90223	0.90223	0.90436
25 mm	0.90233	0.90233	0.90233	0.90444

Table 5
Reaction force (N) results

Bar diameter	S235	50CrV4	AISI 1065	AL 7075
40 mm	5630.90	5631.90	5363.30	1900.90
36 mm	3689.50	3693.80	3521.00	1247.70
34 mm	2958.90	2965.30	2818.20	1013.00
32 mm	2310.80	2310.70	2197.60	784.36
30 mm	1756.70	1760.40	1679.70	593.56
28 mm	1290.00	1290.50	1229.40	422.02
25 mm	843.77	834.91	795.15	306.37

Table 6
Stiffness (Nm/degree) results

Bar diameter	S235	50CrV4	AISI 1065	AL 7075
40 mm	1249.50	1249.73	1190.13	420.75
36 mm	818.48	819.43	781.10	276.11
34 mm	656.14	657.56	624.94	224.09
32 mm	512.47	512.45	487.37	173.53
30 mm	389.47	390.29	372.394	131.28
28 mm	285.96	286.07	272.53	93.33
25 mm	187.02	185.06	176.24	67.75

Table 7
Mass (kg) results

Bar diameter	S235	50CrV4	AISI 1065	AL 7075
40 mm	15.89	15.89	15.89	5.69
36 mm	12.87	12.87	12.87	4.61
34 mm	11.48	11.48	11.48	4.11
32 mm	10.17	10.17	10.17	3.64
30 mm	8.94	8.94	8.94	3.20
28 mm	7.79	7.79	7.79	2.79
25 mm	6.21	6.21	6.21	2.22

Table 8
Safety factor results

Bar diameter	S235	50CrV4	AISI 1065	AL 7075
40 mm	0.88	5.00	1.93	5.56
36 mm	0.99	5.61	2.17	6.24
34 mm	1.07	6.05	2.34	6.73
32 mm	1.11	6.27	2.42	7.06
30 mm	1.20	6.78	2.62	7.54
28 mm	1.29	7.33	2.83	8.15
25 mm	1.48	8.39	3.24	9.36

Table 9
Material performance comparison

	S235	50CrV4	AISI 1065	AL 7075
Rotation	X	X	X	
Reaction force		X		
Stiffness	X	X	X	
Mass				X
Safety factor		X		X
Applicability	X	X	X	X
Cost	X		X	X

Figure 11
Stress distribution result on 36 mm diameter with AISI 1065

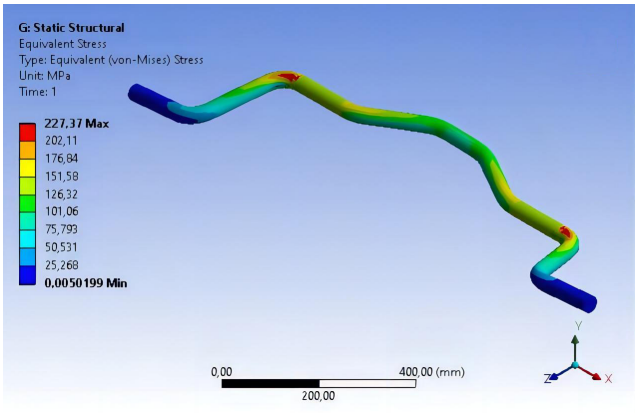

Figure 11 shows the reasonable stress distribution of the anti-roll bar with a diameter of 36 mm and AISI 1065 material according to related studies [4, 9, 22]. As expected, stress occurred at the fillets close to the surface, where the bar was connected to the chassis and had only rotational freedom.

Figure 12 shows the force reaction and torsion angles that occur under the boundary conditions of the distribution seen in Figure 11.

In this study, an optimization of an urban electric bus anti-roll bar was conducted on material and bar diameter. Performance comparison is shared in Table 9, the sign of *X* states a good result

Figure 12
Reaction force (left) and rotation angle (right) results on 36 mm diameter with AISI 1065

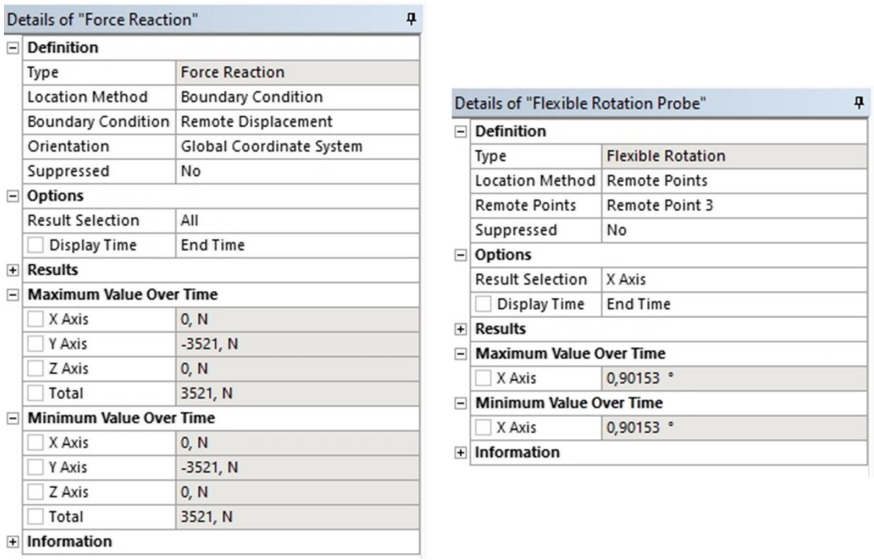

Details of "Force Reaction"	
Definition	
Type	Force Reaction
Location Method	Boundary Condition
Boundary Condition	Remote Displacement
Orientation	Global Coordinate System
Suppressed	No
Options	
Result Selection	All
Display Time	End Time
Results	
Maximum Value Over Time	
X Axis	0, N
Y Axis	-3521, N
Z Axis	0, N
Total	3521, N
Minimum Value Over Time	
X Axis	0, N
Y Axis	-3521, N
Z Axis	0, N
Total	3521, N
Information	

Details of "Flexible Rotation Probe"	
Definition	
Type	Flexible Rotation
Location Method	Remote Points
Remote Points	Remote Point 3
Suppressed	No
Options	
Result Selection	X Axis
Display Time	End Time
Results	
Maximum Value Over Time	
X Axis	0,90153 °
Minimum Value Over Time	
X Axis	0,90153 °
Information	

of material in specified parameter. According to the obtained results, the most effective parameters showed 50CrV4 and AISI 1065 are the most suitable for the anti-roll bar. At this point, the cost of AISI 1065 is more beneficial than 50CrV4 (due to commercial confidentiality, cost data of material supplier was not provided) while 50CrV4 provides better results.

4. Conclusion

Since vehicles are dynamic systems, they are exposed to dynamic loading and therefore structural rigidity has an important place. In this study, the structural rigidity of an anti-roll bar of a bus was examined according to material and diameter changes. Minimum stiffness was determined according to the torsion angle limitation that would occur in response to the targeted lateral acceleration and was considered as the evaluation criterion. As a result of the structural static analyses carried out with S235, 50CrV4, AISI 1065, and AL 7075 materials with diameter values of 40 mm, 36 mm, 34 mm, 32 mm, 30 mm, 28 mm, and 25 mm, the minimum stiffness criteria specified were met with S235, 50CrV4, and AISI 1065 materials with diameters of 40 mm and 36 mm has provided. However, in terms of safety coefficient, combinations with S235 material remained below 1. Combinations with 50CrV4 material are above 5 and are considered extremely safe. The safety coefficient of the remaining AISI 1065 material options was approximately 2, which was found to be a suitable value for an anti-roll bar. In terms of mass, which is the final evaluation criterion, it was observed that the mass values of 40 mm and 36 mm diameter were 15.887 kg and 12.868 kg. The use of 36 mm diameter AISI 1065 material was preferred due to its lightness, sufficient strength, industrial use, and economic conditions.

Since this work provides numerical optimization methods, the results need to be verified with real tests. In future studies, actual anti-roll bar rotation and displacement values will be collected from real driving tests. In parallel, stress values will be obtained using a strain gauge or a suitable tool and FEA results will be verified with real data. In addition, a 1-D model that can numerically simulate the working environment of the anti-roll bar will be created and the model verification will be carried out by transferring the data obtained from the real driving test to the numerical model. A variety of literature will be obtained by performing different optimization methods on the validated 1-D model.

Acknowledgments

The authors specially thank Onur EROL who provided technical support to this study.

Funding Support

The authors would like to thank TUBITAK (Project code 119C154) and KARSAN automotive for their support in the preparation of this study.

Ethical Statement

This study does not contain any studies with human or animal subjects performed by any of the authors.

Conflicts of Interest

The authors declare that they have no conflicts of interest to this work.

Data Availability Statement

Data sharing is not applicable to this article as no new data were created or analyzed in this study.

Author Contribution Statement

Merve Alpar: Software, Validation, Formal analysis, Investigation, Resources, Data curation, Writing – original draft, Writing – review & editing, Visualization. **Efe Savran:** Methodology, Software, Validation, Formal analysis, Investigation, Resources, Data curation, Writing – original draft, Writing – review & editing, Visualization. **Fatih Karpat:** Conceptualization, Methodology, Formal analysis, Writing – original draft, Writing – review & editing, Supervision, Project administration, Funding acquisition.

References

[1] Gao, J., & Wu, F. (2020). The study of optimization and matching to spring and antiroll bar stiffness of suspension for multiresponse target of whole vehicle under sine-swept steering input. *Mathematical Problems in Engineering, 2020*(1), 8820108. https://doi.org/10.1155/2020/8820108

[2] Kumar, Y., Siddiqui, R. A., Upadhyay, Y., & Prajapati, S. (2022). Kinematic and structural analysis of independent type suspension system with anti-roll bar for formula student vehicle. *Materials Today: Proceedings*, *56*, 2672–2679. https://doi.org/10.1016/j.matpr.2021.09.247

[3] Gottschalk, H., & Reese, M. (2021). An analytical study in multi-physics and multi-criteria shape optimization. *Journal of Optimization Theory and Applications*, *189*(2), 486–512. https://doi.org/10.1007/s10957-021-01841-y

[4] Bharane, P., Tanpure, K., Patil, A., & Kerkal, G. (2014). Design, analysis and optimization of anti-roll bar. *Journal of Engineering Research and Applications*, *4*(9), 137–140.

[5] Deshmukhpatil, S. B., & Maskar, P. D. (2021). Design optimization and analysis of composite automotive anti-roll bar. *International Research Journal of Engineering and Technology*, *8*(6), 3746–3752.

[6] Kumar, T. V., Chandrasekaran, M., Padmanabhan, S., Saravanan, R., & Arunkumar, S. (2021). Material and design parameters optimization to enhance the life of anti-roll bar of commercial truck. *Materials Today: Proceedings*, *37*, 1359–1366. https://doi.org/10.1016/j.matpr.2020.06.561

[7] Topaç, M. M., Enginar, H. E., & Kurulay, N. S. (2011). Reduction of stress concentration at the corner bends of the anti-roll bar by using parametric optimisation. *Mathematical and Computational Applications*, *16*(1), 148–158.

[8] Wheatley, G., & Zaeimi, M. (2022). Anti-roll bar design for a formula SAE vehicle suspension. *Scientific Journal of Silesian University of Technology. Series Transport*, *116*, 257–270. https://doi.org/10.20858/sjsutst.2022.116.17

[9] Yachkal, A. K., Nath, N. K., & Khan, S. (2020). Analyses of the effect of clamping distance on stress and roll stiffness of anti roll bar. *International Journal of Applied Engineering Research*, *15*(9), 906–910. https://doi.org/10.37622/ijaer/15.9.2020.906-910

[10] Yang, W., Nong, Z., Bangji, Z., & Jie, Z. (2019). Modeling and performance analysis of a vehicle with kinetic dynamic suspension system. *Proceedings of the Institution of Mechanical Engineers, Part D: Journal of Automobile Engineering*, *233*(3), 697–709. https://doi.org/10.1177/0954407017748281

[11] van Puymbroeck, E., Nagy, W., Schotte, K., Ul-Abdin, Z., & de Backer, H. (2019). Determination of residual welding stresses in a steel bridge component by finite element modeling of the incremental hole-drilling method. *Applied Sciences*, *9*(3), 536. https://doi.org/10.3390/app9030536

[12] Baughman, J. A. (2023). *Introduction to mechanical engineering design*. USA: Iowa State University Digital Press. https://doi.org/10.31274/isudp.2023.131

[13] Valsamos, G., Larcher, M., Casadei, F., & Karlos, V. (2020). *A numerical framework to support the certification of barrier testing*. Luxembourg: Publications Office of the European Union. https://doi.org/10.2760/797952

[14] Topaç, M. M., & Kuralay, N. S. (2009). Yolcu otobüsü stabilizatörünün bilgisayar destekli tasarımı [Computer-aided design of a passenger bus stabilizer]. *Mühendis ve Makina*, *50*(594), 14–24.

[15] Ning, Z., Gao, Y., & Wang, A. (2020). Design and performance analysis of a new optimization algorithm based on finite element analysis. *Science Progress*, *103*(3), 0036850420950852. https://doi.org/10.1177/0036850420950852

[16] Savran, E., Vargelci, S., Catenaro, L., & Karpat, F. (2022). Otomobil ön tampon braketinde tasarım İyileştirmesi [Design improvement to the automobile front bumper bracket]. *Avrupa Bilim ve Teknoloji Dergisi*, (45), 120–125. https://doi.org/10.31590/ejosat.1219759

[17] Savran, E., Vargelci, S., Catenaro, L., & Karpat, F. (2023). Bİr otomobİl braket tasariminin analİzİ ve değerlendİrmesİ [Mechanical assessment of an automobile bracket]. *Uludağ University Journal of the Faculty of Engineering*, *28*(2), 493–506. https://doi.org/10.17482/uumfd.1299676

[18] Sadek, M., Bergström, J., Hallbäck, N., Burman, C., Elvira, R., & Escauriaza, B. (2020). Fatigue strength and fracture mechanisms in the very-high-cycle-fatigue regime of automotive steels. *Steel Research International*, *91*(8), 2000060. https://doi.org/10.1002/srin.202000060

[19] Abdellah, M. Y., Hassan, M. K., Al-Shwihi, M. M., Backar, A. H., & Mohamed, A. F. (2021). CAD design of Arcan fixture and finite element simulation based on stress analysis for optimum shear mode. *Journal of Mechanical Engineering Research and Developments*, *44*(2), 185–197.

[20] Zhang, H., Wu, Z., & Xu, Q. (2020). Design of a new XY flexure micropositioning stage with a large hollow platform. *Actuators*, *9*(3), 65. https://doi.org/10.3390/ACT9030065

[21] Hwang, H.-Y., Lan, T.-S., & Chen, J.-S. (2020). Developing a strategy to improve handling behaviors of a medium-size electric bus using active anti-roll bar. *Symmetry*, *12*(8), 1334. https://doi.org/10.3390/sym12081334

[22] Bhanage, A., & Padmanabhan, K. (2015). Static and fatigue simulation of automotive anti roll bar before DBTT. *International Journal of Applied Engineering Research*, *10*(71), 472–476.

How to Cite: Alpar, M., Savran, E., & Karpat, F. (2026). Anti-roll Bar Optimization of an Urban Electric Bus. *Archives of Advanced Engineering Science*, *4*(1), 25–32. https://doi.org/10.47852/bonviewAAES42022250